



137  
503  
THS

MSU  
1  
003  
359341



This is to certify that the  
thesis entitled

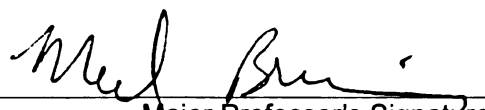
Size-selective Transport of Uncharged Solutes through  
Multilayer Polyelectrolyte Membranes

presented by

Xiaoyun Liu

has been accepted towards fulfillment  
of the requirements for the

M.S. degree in chemistry

  
Major Professor's Signature

8/13/03

Date

**PLACE IN RETURN BOX** to remove this checkout from your record.  
**TO AVOID FINES** return on or before date due.  
**MAY BE RECALLED** with earlier due date if requested.

DATE DUE	DATE DUE	DATE DUE

**Size-selective Transport of Uncharged Solutes  
through Multilayer Polyelectrolyte Membranes**

By

Xiaoyun Liu

A THESIS

Submitted to  
Michigan State University  
in partial fulfillment of the requirements  
for the degree of

MASTER OF SCIENCE

Department of Chemistry

2003

## **Abstract**

### **Size-selective Transport of Uncharged Solute through Multilayer Polyelectrolyte Membranes**

By

Xiaoyun Liu

Several recent studies demonstrated highly selective ion transport through multilayer polyelectrolyte membranes. This thesis examines the transport of neutral molecules through multilayer polyelectrolyte films and shows significant size-based discrimination among organic analytes. Simple 7-bilayer poly(styrene sulfonate) (PSS)/poly(allylamine hydrochloride) (PAH) films deposited on porous alumina exhibit a glucose/sucrose selectivity of  $\sim 150$  in both diffusion dialysis and nanofiltration. However, selectivity among smaller solutes is fairly low (methanol/glycerol  $\approx 2$  and glycerol/glucose  $\approx 8$ ). High selectivity in nanofiltration by PSS/PAH membranes is accompanied by relatively high solute rejections. Although such high rejections will preclude the use of these membranes in sugar separations, they may prove useful in applications such as removal of organic pollutants from water. The high water flux through PSS/PAH films ( $0.9 \text{ m}^3 \text{ m}^{-2} \text{ d}^{-1}$  at 4.8 bar) would also be important in water purification. Capping PSS/PAH films with a few bilayers of poly(acrylic acid) (PAA)/PAH increases glycerol/glucose diffusion-dialysis selectivity from 8 to 75. Thus, controlling film composition may allow tailoring of membrane properties for specific separations. Simulations of nanofiltration and diffusion dialysis data for 7-bilayer PSS/PAH membranes suggest that these films have a porosity of 2 to 3% and pores with radii of 0.4 to 0.5 nm.

## **ACKNOWLEDGEMENTS**

First of all, I want to thank my advisor, Dr. Bruening. I have really enjoyed the two years' research under your guidance. Being with you is a great pleasure and working with you is a process of having fun. I am impressed by your thoughtful insight into scientific problems, your determination to figure out any puzzle, your great sense of humor and.... Thank you so much.

Also, I would like to thank all my group members, past and present. Jinhua, Yingda, and Wenxi, thank you so much for helping me get through the hard times. A smart guy, Dan, I want to thank you for your help on technical problems, both for me and for the group. Anagi, Bo, Brian, Christin, Jin, Keith, Lei, Mat, and Sri, nice to work with you.

Last, I want to thank my loved parents and sister on the other side of the earth (I miss you so much), and all my loved friends both here and in China. I am here because of all of you!

# TABLE OF CONTENTS

List of Tables	v
List of Figures	vi
<b>Chapter 1. Introduction and Background</b>	<b>1</b>
1.1 Membranes	1
1.2 Introduction to Membrane Processes	2
1.3 Nanofiltration: Significance and Applications	5
1.4 Ultrathin Organic Films and Multilayer Polyelectrolyte Membranes	6
1.5 Transport through Porous and Nonporous Membranes	10
1.6 Motivation behind this Research	17
 <b>Chapter 2. Size-selective Transport of Uncharged Solutes through Multilayer Polyelectrolyte Membranes</b>	 <b>19</b>
2.1 Introduction	19
2.2 Experimental Section	20
2.2.1 Materials	20
2.2.2 Film Deposition	20
2.2.3 Transport Studies	21
2.3 Results and Discussion	27
2.3.1 Diffusion Dialysis through PSS/PAH Membranes	27
2.3.2 Diffusion Dialysis through Hybrid PSS/PAH/PAA Membranes	31
2.3.3 Nanofiltration with PSS/PAH Membranes	34
2.3.4 Theory for Modeling of Transport	37
2.3.5 Determination of Effective Pore Sizes	42
 <b>Chapter 3. Conclusions and Future Work</b>	 <b>46</b>
<b>References</b>	<b>47</b>

## LIST OF TABLES

Table 1. Typical Pressures, Permeabilities, and Solute Sizes Associated with Different Pressure-driven Membrane Separations	4
Table 2. Molecular Weights, Diffusion Coefficients (D) and Stokes' Radii ( $r_s$ ) of Several Neutral Solutes	18
Table 3. Normalized Fluxes ( $\text{mol cm}^{-2} \text{ s}^{-1} / \text{M}$ ) and Selectivities in Diffusion Dialysis through Bare Porous Alumina and Alumina Coated with Polyelectrolyte Films	30
Table 4. Percent Rejections, Water Fluxes (in $\text{m}^3 \text{m}^{-2} \text{d}^{-1}$ ), and Selectivities from NF Experiments with Multilayer Polyelectrolyte Membranes and Solutions Containing Several Neutral Molecules	35
Table 5. Parameters and Fluxes ( $\text{mol cm}^{-2} \text{ s}^{-1}$ ) Relevant to the Simulation of Diffusion Dialysis through a 7-bilayer PSS/PAH Membrane Assuming a Membrane Pore Radius of $5.28 \times 10^{-8} \text{ cm}$	43
Table 6. Parameters and Rejections Calculated in the Simulation of Nanofiltration with a 7-bilayer PSS/PAH Membrane Assuming a Membrane Pore Radius of $4.2 \times 10^{-8} \text{ cm}$	43



## LIST OF FIGURES

Figure 1. Schematic representation of a membrane-based separation process.	3
Figure 2. Schematic diagram of layer-by-layer deposition of oppositely charged polyelectrolytes on a porous substrate.	8
Figure 3. Krasemann and Tieke model for rejection of several different ions by a multilayer polyelectrolyte film.	10
Figure 4. Some characteristic pore geometries found in porous membranes.	11
Figure 5. Schematic representation of the cell used in diffusion dialysis.	22
Figure 6. Schematic diagram of the cross-flow nanofiltration apparatus.	23
Figure 7. Gas-chromatography calibration curve for methanol.	25
Figure 8. Typical chromatogram of glycerol (peak 1), glucose (peak 2) and sucrose (peak 3) in LC analysis.	26
Figure 9. Normalized permeate-phase concentrations of glycerol (squares), glucose (triangles), and sucrose (diamonds) as a function of time in diffusion dialysis through a 7-bilayer PSS/PAH membrane. The inset shows an expanded view for glucose and sucrose.	28
Figure 10. Normalized permeate-phase concentrations of methanol (squares), glycerol (triangles), and glucose (diamonds) as a function of time in a diffusion dialysis experiment with a 5-bilayer PSS/PAH + 1.5-bilayer PAA/PAH film. The inset shows the expanded view of glycerol and glucose transport across the membrane.	32
Figure 11. Schematic diagram of the analyte concentration profile in a membrane composed of a polyelectrolyte film on a porous alumina support.	38

# **Chapter 1**

## **Introduction and Background**

### **1.1 Membranes**

A membrane is defined as a selective barrier between two phases. These barriers can be thick or thin, and their structure can be homogeneous or heterogeneous. Additionally, membranes can be natural or synthetic, neutral or charged. Although membranes can be classified from different points of view, morphological classification is probably most pertinent to this thesis. Generally speaking, there are two types of membrane structures: symmetric and asymmetric. Symmetric membranes consist of a homogeneous film whose thickness is generally relatively large (10 to 200  $\mu\text{m}$ ). Because flux through a membrane is usually inversely proportional to membrane thickness, transport through symmetric membranes is often unacceptably slow.

The development of asymmetric membranes revolutionized industrial applications of membranes. These structures consist of a very dense skin layer (thickness of 0.1 to 0.5  $\mu\text{m}$ ) on a porous substrate (thickness of 50 to 150  $\mu\text{m}$ ). The skin layer provides selectivity, while the porous support affords mechanical stability.<sup>1,2</sup> Even though the skin layer may be highly size-selective, its minimal thickness still allows high flux. Because the support is highly porous, resistance to mass transfer is largely determined by the thin skin layer.

## 1.2 Introduction to Membrane Processes

Membrane processes are designed to achieve specific separations. Paramount in any process is the capability of the membrane to allow faster transport of one component than another. Differences in transport rates result from differences in physical (size) or chemical properties of the transporting compounds. Driving forces behind transport include electrical potentials, pressure, and concentration gradients (Figure 1). Usually the transport rate, or solute flux, is proportional to the driving force. For instance, in diffusion dialysis, the flux is proportional to the concentration gradient as shown by Fick's law (equation 1).

$$j_i = -D_i \frac{dc_i}{dx} \quad (1)$$

In this equation,  $j_i$  represents solute flux,  $D_i$  is the solute diffusion coefficient in the membrane, and  $dc_i/dx$  is the concentration gradient.

Membrane-based separations are applied in a wide variety of processes including: microfiltration (MF), ultrafiltration (UF), nanofiltration (NF), reverse osmosis (RO), electrodialysis, diffusion dialysis, gas separation, pervaporation and membrane distillation. Among these processes, MF, UF, NF, and RO are all pressure-driven processes that involve the separation of solutes. Classification of these processes is generally based on solute size and operating pressure. For the sake of comparison, Table 1 lists the solute sizes, operating pressures, and membrane permeabilities in MF, UF, NF, and RO.

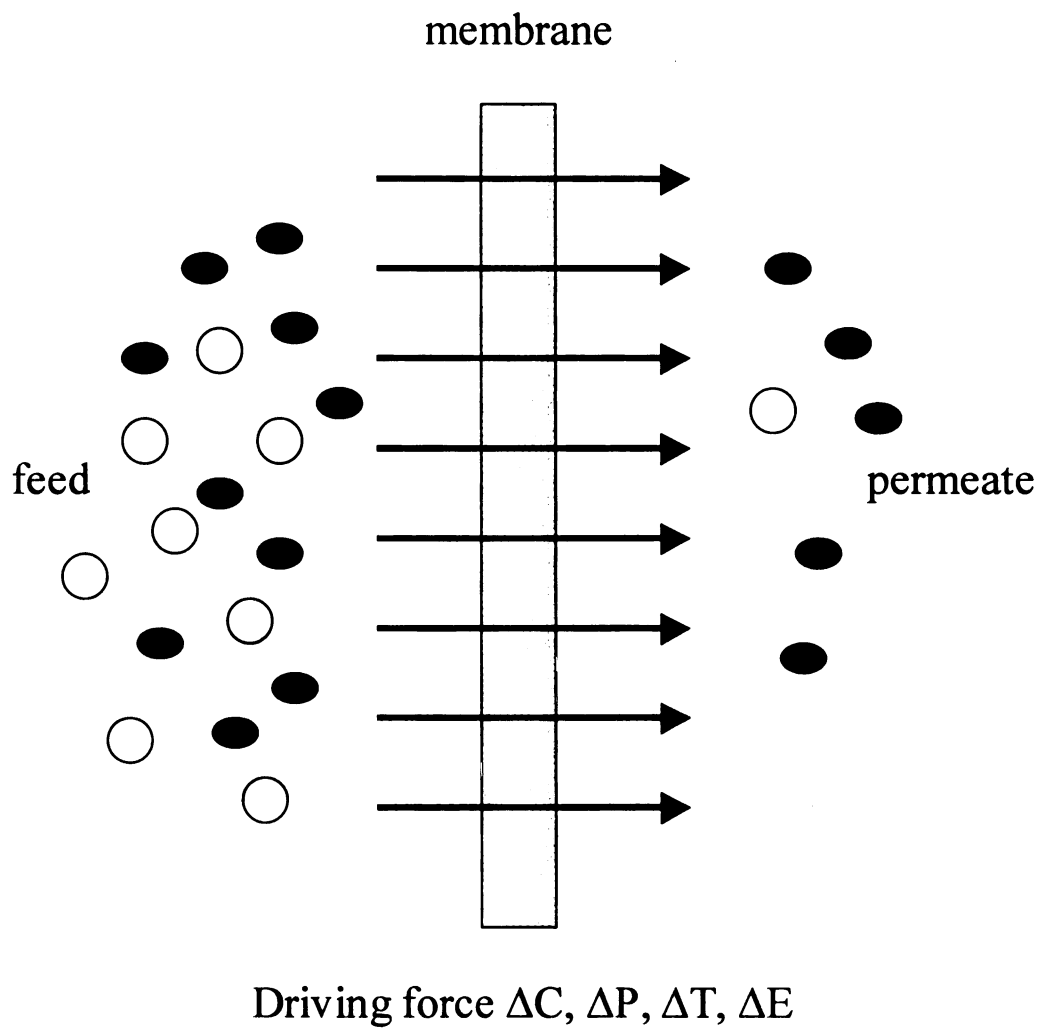


Figure 1. Schematic representation of a membrane-based separation process.

**Table 1. Typical Pressures, Permeabilities, and Solute Sizes Associated with Different Pressure-driven Membrane Separations<sup>3</sup>**

membrane process	pressure range (bar)	permeability (L m <sup>-2</sup> h <sup>-1</sup> bar <sup>-1</sup> )	solute size (nm)
microfiltration	0.1-2.0	>50	>100
ultrafiltration	1.0-5.0	10-50	5-100
nanofiltration	5.0-20	1.4-12	0.1-8
reverse osmosis	10-100	0.05-1.4	<1

Application requirements generally dictate membrane structure.<sup>3</sup> For example, retention of particles with diameters >100 nm (microfiltration) can occur with a highly porous structure, while separation of macromolecules (molecular weights ranging from about 10<sup>4</sup> to more than 10<sup>6</sup>) in ultrafiltration necessitates somewhat denser membranes. Separation of low molecular weight compounds in applications such as pervaporation and gas separation calls for the use of dense, nonporous membrane materials. NF and RO membranes, which are employed for separation of inorganic ions or small organic molecules from solvent, have a structure that is intermediate between open, porous membranes (MF/UF) and dense, nonporous membranes (pervaporation and gas separation).

### **1.3 Nanofiltration: Significance and Applications**

Nanofiltration (NF) is becoming an increasingly important membrane process for separations in areas such as water purification, treatment of pulp and paper mill effluents, fractionation/purification of protein, cheese-whey desalting, and sulfate removal from oil-well injection water.<sup>4</sup> Since the properties of NF membranes fall between those of UF and RO systems, the separation mechanism in NF can involve both steric (sieving) and electrical (Donnan) effects. The electrical effect can play a very important role in electrolyte separations. However, for neutral molecules such as sugars, mass transport through NF membranes is controlled primarily by steric factors.<sup>5</sup> The advantage of NF over RO is operation at moderate pressures along with a relatively high flux. Thus, in applications such as water softening, NF membranes can provide purified water at a lower operating cost. However, analytes separated by NF are generally larger than those separated by RO. NF membranes can remove essentially 100% of suspended particles, but they will not remove as many dissolved substances as RO membranes, especially small inorganic ions like  $\text{Na}^+$  and  $\text{Cl}^-$ . One can think of a NF membrane as a more “porous” RO system, although according to the “solution-diffusion” theory often applied to RO membranes, there are no actual “pores”.

The largest users of NF technology are municipal drinking water plants, and the state of Florida is, by far, the greatest user of NF in the United States. It is estimated that Florida NF operations will soon be capable of producing more than 100 million

gallons per day of NF permeate.<sup>6</sup> There are existing plants that process more than 10 million gallons of water per day.

#### **1.4 Ultrathin Organic Films and Multilayer Polyelectrolyte Membranes (MPMs)**

The key to further enhancing the utility of NF is the development of membranes that exhibit high flux and selectivity as well as durability and resistance to fouling.<sup>7,8</sup> Synthesis of such membranes typically requires formation of an ultrathin, defect-free film on a highly permeable support in order to achieve sufficient fluxes in highly selective systems.<sup>1,2,9-11</sup> However, conventional techniques of film preparation are not capable of forming ultrathin, defect-free separating layers. Solution casting, for example, is limited to the preparation of layers with thicknesses  $> 1 \mu\text{m}$ .<sup>12</sup> Preparation of thinner separating layers requires more sophisticated deposition techniques. In this regard, methods that allow thickness control at the nanometer level, (e.g., self-assembly and Langmuir-Blodgett (LB) techniques<sup>13-17</sup>) would clearly be advantageous. More than 20 years ago, researchers tried to prepare composite membranes using the LB technique to deposit multilayers of amphiphiles or amphiphilic polymers on porous supports.<sup>18</sup> However, the LB separation layers did not provide high permeability and selectivity because they consisted of densely packed aliphatic chains with poor molecular mobility and low flexibility. Even the use of amphiphilic polymers with short alkyl side groups did not substantially improve the separation efficiency. More recently, Regen and coworkers employed calixarene amphiphiles to form selective membranes by the LB technique.<sup>16</sup> Although Regen's

membranes are very impressive, fabrication of these materials on a large scale will likely be very difficult.

About a decade ago, Decher and co-workers<sup>19-21</sup> reported preparation of thin polymer films using electrostatic layer-by-layer assembly of cationic and anionic compounds on a solid substrate. In a typical process, a negatively charged substrate is dipped into a dilute aqueous solution of a positively charged polyelectrolyte so that the polymer adsorbs on the substrate surface to form a molecularly thin film and reverse surface charge. After careful washing, the coated substrate is dipped into an aqueous solution of a negatively charged polyelectrolyte so that this polymer adsorbs on top of the previous one and again reverses surface charge. Repetition of the adsorption steps yields a polyelectrolyte multilayer assembly in a simple, environmentally clean, and elegant procedure.

Soon after the first report on molecular films prepared by alternating polyelectrolyte deposition (APD), Stroeve and co-workers<sup>22</sup> applied this technique to the preparation of composite membranes. Polyelectrolytes were successively adsorbed on hydrophilized, porous surfaces to form a skin layer as schematically outlined in Figure 2. Films prepared by APD are attractive materials for membrane skins for several reasons. First, their minimal thickness should allow high fluxes.<sup>23</sup> Film thickness can be controlled on the nanometer scale simply by varying the number of deposited bilayers. Second, nearly any polyelectrolyte can form these films, and thus one can easily tune a separation through proper selection of film constituents.<sup>24-31</sup> In addition, variation of deposition conditions such as solution



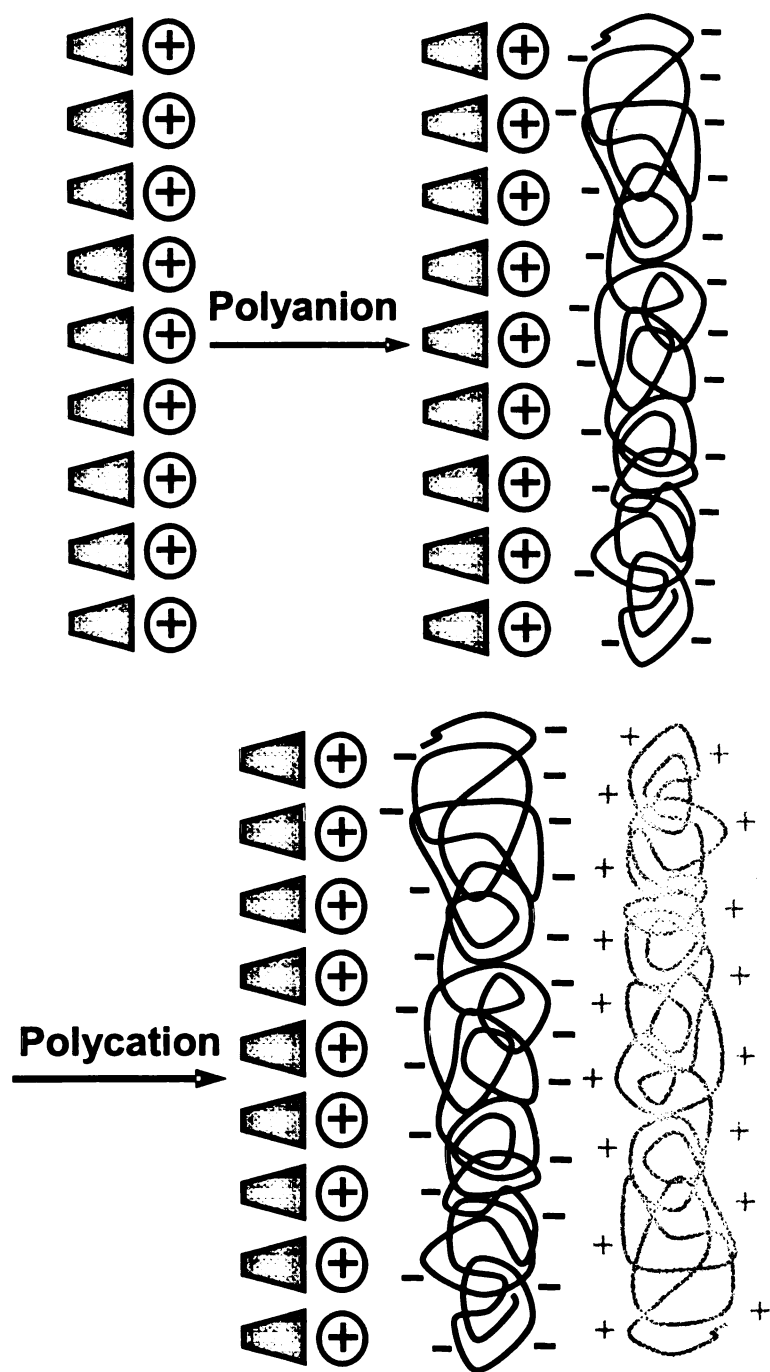


Figure 2. Schematic diagram of layer-by-layer deposition of oppositely charged polyelectrolytes on a porous substrate.

pH<sup>32-34</sup> and supporting electrolyte concentration<sup>35-38</sup> also allows optimization of film properties. Finally, recent studies suggest that some polyelectrolyte films resist cell growth and protein adhesion and thus, may be somewhat resistant to fouling.<sup>39,40</sup>

Over the past few years, a number of groups examined the capabilities of multilayer polyelectrolyte membranes (MPMs) in gas separation,<sup>22,41-43</sup> pervaporation separation of alcohol/water mixtures,<sup>44-46</sup> and microfiltration of protein solutions<sup>47-49</sup>. Additionally, MPMs are especially attractive for separating ions with different valences.<sup>50-54</sup> Krasemann and Tieke demonstrated  $\text{Cl}^-/\text{SO}_4^{2-}$  selectivity as high as 45 using poly(allylamine hydrochloride) (PAH)/poly(styrene sulfonate) (PSS) films and suggested that selectivity is due to greater Donnan exclusion of the divalent  $\text{SO}_4^{2-}$ .<sup>53</sup> Their model of ion rejection,<sup>53</sup> which is represented in Figure 3, implies that ion separation should become progressively more effective as the number of adsorbed polyelectrolyte layers increases. However, fundamental studies of polyelectrolyte films suggest that polycations and polyanions are highly intertwined and that the bulk of these films does not contain a layered structure. Farhat and Schlenoff showed that diffusion through multilayer polyelectrolyte films on electrodes depends on analyte charge,<sup>55,56</sup> and we recently reported enhancement of the ion-transport selectivity of MPMs through cross-linking, hybridization, and control over charge density.<sup>51,57-59</sup> Preliminary simulations suggest that both selective diffusion and Donnan exclusion play a role in effecting selectivity. Donnan exclusion occurs primarily at the film surface.

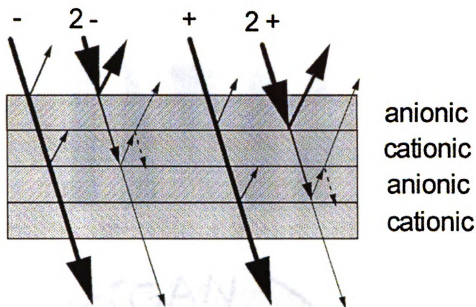


Figure 3. Krasemann and Tieke model for rejection of several different ions by a multilayer polyelectrolyte film (Taken from reference 52, with permission from the American Chemical Society, copyright 2000).

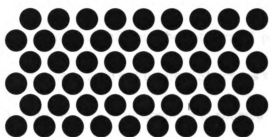
### 1.5 Transport through Porous and Nonporous Membranes.

Figure 4 gives a schematic representation of several geometries that are possible in porous membranes. The particular geometry in a membrane must be taken into account in any model of transport. However, if pore geometry is approximately known, transport models can demonstrate which structural parameters govern flux and suggest how to improve membrane performance.

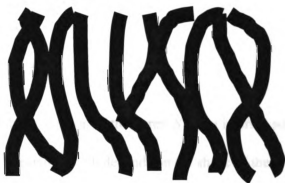
The simplest representation of pore geometry is an assembly of parallel cylindrical pores that extend completely through the membrane (see Figure 4a). Assuming that all the pores have the same radii,  $r$ , equation (2) provides an expression for volume flux,  $J_v$ , through a membrane.



(a)



(b)



(c)

Figure 4. Some characteristic pore geometries found in porous membranes.<sup>3</sup>

$$J_v = \frac{r^2 \epsilon \Delta P}{8 \eta \tau \Delta x} \quad (2)$$

This equation shows that solvent flux is proportional to the driving force, i.e. the pressure drop ( $\Delta P$ ) across the membrane, and inversely proportional to the solution viscosity,  $\eta$ , and the membrane thickness  $\Delta x$ . Other variables that affect flux include membrane porosity ( $\epsilon$ ), which is the fractional pore area, and  $\tau$ , which is the pore tortuosity. (For cylindrical pores, the tortuosity is equal to unity)

The Hagen-Poiseuille equation (equation (2)) gives a good description of transport through membranes consisting of a number of parallel pores. However, very few practical membranes possess such a structure. Structures similar to a system of closed packed spheres (Figure 4b), are more common in sintered inorganic membranes or in the nodular top layer of membranes prepared by phase inversion. The Kozeny-Carman relationship describes the volume flux through such membranes as shown in equation (3),<sup>3</sup>

$$J_v = \frac{\epsilon^3}{K \eta S^2 (1 - \gamma)^2} \frac{\Delta P}{\Delta x} \quad (3)$$

where  $\gamma$  is the volume fraction of the pores,  $S$  is the internal surface area and  $K$  is the Kozeny-Carman constant, which depends on the shape of the pores and the tortuosity.

Some membranes prepared by phase inversion have a sponge-like structure, as schematically shown in Figure 4c. Either the Hagen-Poiseuille or the Kozeny-Carman relationship can describe the volume flux through these membranes, although the morphologies implied by the two models are quite different.

Nonporous materials constitute another important class of membranes. When the

sizes of molecules to be separated are in the same order of magnitude as oxygen, nitrogen or hexane, porous membranes cannot effect a separation, and nonporous membranes are necessary. However, the term nonporous is rather ambiguous because pores (permanent or transient) must be present on a molecular level or no transport would occur. Free volume theory provides a good description of the existence of dynamic molecular pores and allows modeling of diffusion coefficients in non-porous membranes. The solution-diffusion mechanism describes the overall process of transport through nonporous materials and satisfactorily explains the transport of gas, vapor or liquid through a dense, nonporous membrane. This is also the most popular model for reverse osmosis systems. Equations (4) and (5) comprise the essence of the solution diffusion model. Flux is proportional to the permeability coefficient,  $P$ , and the pressure drop across the membrane,  $\Delta p$ , and inversely proportional to the membrane thickness,  $\Delta x$ . The permeability coefficient is a function of the solubility coefficient,  $S$ , for a transporting species as well as the diffusion coefficient,  $D$ , of this species.

$$\text{Flux } (j) = \text{Permeability } (P) \times \Delta p / \Delta x \quad (4)$$

$$\text{Permeability } (P) = \text{Solubility } (S) \times \text{Diffusivity } (D) \quad (5)$$

The solubility coefficient is a thermodynamic parameter and gives a measure of the amount of solute absorbed by the membrane under equilibrium conditions. Henry's law applies to the low solubility of gases in elastomeric polymers, and  $S$  is a constant. However, with organic vapors or liquids, which are not as ideal as permanent gases,  $S$  is a more complicated function of concentration. Diffusivity is a kinetic parameter

that indicates how fast a solute transports through the membrane. The diffusion coefficient depends on the geometry of the solute and decreases with increasing solute size. For solutes that are capable of swelling the membrane, diffusion coefficients will also depend on concentration.

Quantitative methods for predicting performance in membrane-based separations will facilitate the optimization of existing systems and broaden the range of membrane applications. Modeling of transport requires data that describe membrane properties as well as a fundamental mathematical description of the transport process. This thesis focuses on NF, and the properties of NF membranes required for simulations include pore density and geometry and electrical parameters such as the surface charge density or the volumetric charge density. Since NF membranes have nm-sized pores, and macroscopic descriptions of hydrodynamics may fail at these dimensions, it is especially challenging to decide whether to model these membranes as porous or dense, homogeneous materials. The assumption of a porous membrane necessitates the description of solute transport inside pores with radii that are only a few times larger than the radii of water molecules. This, in turn, leads to the question of whether one can truly apply macroscopic descriptions of hydrodynamic and charge interactions to NF membranes. Providing an answer to this question is difficult because no existing analytical or physical techniques can probe the structure of NF membranes with confidence. Most models of transport through NF membranes have thus far assumed such membranes to consist of bundles of capillary tubes. Essentially, the macroscopic models that were used for large pores have been adapted to describe NF.

The extended Nernst-Planck equation (equation (6)) forms the basis for modeling the flux,  $j_i$ , of ions and neutral solutes through porous membranes. In this equation,

$$j_i = -D_i \frac{dc_i}{dx} - \frac{z_i c_i D_i}{RT} F \frac{d\psi}{dx} + c_i J_v \quad (6)$$

diffusive flux is proportional to the diffusion coefficient,  $D_i$ , and the concentration gradient,  $dc_i/dx$ , while flux due to migration is proportional to the potential gradient,  $d\psi/dx$ , solute charge,  $z_i$ , solute concentration,  $c_i$ , the diffusion coefficient,  $D_i$ , and several standard fundamental constants. The convective term, which is proportional to the volume flux of solvent,  $J_v$ , and the solute concentration,  $c_i$ , represents solute being dragged through the membrane with solvent. When coupled with a suitable description of the partitioning of solutes between solution and membrane, the extended Nernst-Planck equation provides a complete description of transport. For uncharged solutes, only the diffusive and convective flows contribute to transport, so the expression for flux can be simplified to equation (7).

$$j_i = -D_i \frac{dc_i}{dx} + c_i J_v \quad (7)$$

In the case of very small pores, both diffusion and convection are hindered by drag of the solute on the pore wall. Bowen and Mukhtar accounted for the hindered nature of diffusion and convection of the solutes inside the membrane with the terms  $K_{i,d}$  and  $K_{i,c}$ , respectively, in equation (8).

$$j_i = -K_{i,d} D_i \frac{dc_i}{dx} - \frac{z_i c_i K_{i,d} D_i}{RT} F \frac{d\psi}{dx} + K_{i,c} c_i J_v \quad (8)$$

These hindrance factors are often calculated using the hydrodynamic coefficients  $K^l$ , the enhanced drag, and  $G$ , the lag coefficient, for a spherical solute moving inside a cylindrical pore of infinite length.



A number of previous studies examined transport models for NF membranes. The separation of charged solutes in NF membranes has been interpreted using the extended Nernst-Planck equation combined with the Teorell-Meyer-Sievers assumption (TMS model)<sup>60-62</sup> or the space-charge pore (SCPM) model.<sup>62</sup> The TMS model assumes that the membrane is homogenous, that the distribution of fixed charge density inside the membrane is uniform and that ion transport may be quantified using bulk diffusivities. Donnan equilibrium is employed to calculate concentrations at membrane-solution interfaces. Wang et al.<sup>63</sup> employed the TMS model to estimate the effective charge density in several NF membranes by using the effective thickness/porosity values obtained from separate experiments on uncharged solutes. The SCPM model takes into account the charge distribution inside of small pores as well as the Poiseuille flow profile.

Bowen and Mukhtar<sup>64</sup> proposed a hybrid model based on the extended Nernst-Planck equation to describe the transport of salts. The model assumed that the membranes were homogenous but included hindrance factors for diffusion and convection (mentioned above) to allow for the transport of ions in the membrane taking place within a confined space. The effective pore radius was estimated by fitting the rejection data for Na<sub>2</sub>SO<sub>4</sub> and NaCl. In a subsequent paper, Bowen et al.<sup>65</sup> used a similar model to interpret experimental data for the rejection of three salts with a common co-ion and five uncharged solutes. Additionally, they attempted to make direct measurements of surface pore radius and surface porosity by AFM. Comparison of the results of these techniques allowed an evaluation of the

appropriateness and applicability of three possible descriptions of transport and rejection in NF membranes i.e. a hybrid model (HM) without a solute velocity distribution in pores, a porous flow model (radial variation in velocity within a pore) (PM), and a pore model with a full description of the space charge in the pores (SCPM). Comparison of the characterization parameters obtained with HM and PM models with salts and uncharged solutes suggested that PM gave results in better agreement than the HM. It was probably due to the fact that the derivation of hindrance factors inherently assumed a velocity distribution of the solute inside the pores. Additionally, calculations of the potential distribution across pores indicated that the variation of potential is less than 3 mV for membranes with a pore radius  $< 2.0$  nm. Thus, for most nanofiltration membranes, the added complexity of the SCPM model which describes the potential distribution is not necessary.

## **1.5 Motivation behind this Research**

The main objective of this work is to better understand transport through multilayer polyelectrolyte films by studying the diffusion of various neutral molecules across MPMs. The use of neutral analytes eliminates Donnan effects and allows us to focus exclusively on size-based selectivity. In addition to providing fundamental insight, neutral molecule studies will be important for potential applications of MPMs such as controlled release,<sup>66-71</sup> water purification,<sup>72,73</sup> and salt/sugar separations.<sup>74,75</sup> We chose to investigate transport of methanol, glycerol, glucose, and sucrose because these molecules differ in size (Table 2) and yet have similar functional groups and

hydrophilicities.<sup>65,76</sup> Diffusion dialysis studies with these molecules show that MPMs can exhibit very high size-based selectivities (glucose/sucrose selectivity reaches 150) that depend on membrane composition. Selectivities are maintained in high-flux NF, but rejections are also high. Even with the smallest molecule, methanol, rejection by PSS/PAH films is 70%. These high rejections suggest that PSS/PAH membranes may be useful in removal of organic pollutants from water.

**Table 2. Molecular Weights, Diffusion Coefficients (D) and Stokes' Radii (r<sub>s</sub>) of Several Neutral Solutes<sup>65,77</sup>**

solute	MW	D (m <sup>2</sup> s <sup>-1</sup> × 10 <sup>-9</sup> )	r <sub>s</sub> (nm)
methanol	32	1.56	0.157
glycerol	92	0.95	0.260
glucose	180	0.69	0.355
sucrose	342	0.52	0.471

## **Chapter 2**

### **Size-selective Transport of Uncharged Solutes through Multilayer Polyelectrolyte Membranes**

#### **2.1 Introduction**

Recently, several studies demonstrated that alternating electrostatic adsorption of cationic and anionic polyelectrolytes on porous supports is a versatile method to prepare composite membranes with an ultrathin, defect-free separation layer.<sup>22,23,33,52</sup> Careful choice of the polyelectrolytes and the porous substrate and optimization of processing parameters afford composite membranes that exhibit high ion-transport selectivities as well as high flux. However, transport through polyelectrolyte films is still not well understood, partly because ion-transport selectivity is determined by both size and electrostatic exclusion. Through studying the transport of several neutral molecules, this work shows that typical poly(styrene sulfonate) (PSS)/poly(allylamine hydrochloride) (PAH) membranes have pore sizes of 0.4-0.5 nm. Glucose/sucrose selectivity through these films is about 150, but size-selectivities among molecules with sizes similar to common inorganic ions are minimal. In addition to providing fundamental insight about pores in multilayer polyelectrolyte films, this thesis reports nanofiltration experiments that suggest that PSS/PAH films may be useful for removing organic pollutants from water or for separation of salts from sugars.

## 2.2 Experimental Section

**2.2.1 Materials.** Poly(styrene sulfonate) (PSS) (Aldrich, Mw = 70,000), poly(allylamine hydrochloride) (PAH) (Aldrich, Mw = 70,000), poly(acrylic acid) (PAA) (Mw = 90,000, 25 wt % solution, Alfa Aesar), MnCl<sub>2</sub> (Mallinckrodt), NaBr (Aldrich), NaCl (Mallinckrodt), methanol (CCI, ACS grade, anhydrous), glycerol (CCI, ACS grade, anhydrous), glucose (Aldrich), and sucrose (Aldrich) were used as received. The porous alumina supports (Anodisc 0.02  $\mu$ m membrane filters) were purchased from Whatman and subjected to UV/O<sub>3</sub> cleaning (Boeckel UV\_Clean model 135500) for 15 min before film deposition. Deionized water (Milli-Q, 18.2 M $\Omega$ cm) was used for rinsing and preparation of the polyelectrolyte solutions. The pH of polyelectrolyte solutions was adjusted with dilute NaOH or HCl.

**2.2.2 Film Deposition.** A cleaned porous alumina support was first placed in an O-ring holder so that only the top of substrate would be exposed to polyelectrolyte solutions. Polyelectrolyte deposition began with immersion of the alumina support in 0.02 M PSS (pH 2.1, 0.5 M MnCl<sub>2</sub>) for 2 min. (Polymer concentrations are always given with respect to the repeating unit.) The substrate was rinsed with deionized water for 1 min before a 5-min immersion in 0.02 M PAH (pH 2.3, 0.5 M NaBr for PSS/PAH bilayers and pH 4.5, 0.5 M NaCl for PAA/PAH bilayers) and subsequent rinsing. Additional bilayers were deposited similarly. Supporting electrolytes and pH values were chosen to follow literature procedures.<sup>2,34,78</sup> Capped films were synthesized through deposition of a 5-bilayer PSS/PAH film followed by deposition of PAA/PAH.

The PAA deposition step involved a 5-min immersion in 0.02 M PAA (pH 4.5, 0.5 M NaCl). Films were dried with N<sub>2</sub> only after deposition of all layers.

**2.2.3 Transport Studies.** A home-built dialysis apparatus (see Figure 5) was used to study the transport of neutral molecules. The apparatus consists of two glass cells (100 mL) connected by a 2.5-cm-long neck in which the membrane was sandwiched between the feed and permeate sides. The exposed membrane area was 2.3 cm<sup>2</sup>, and both feed and permeate sides were stirred vigorously to minimize concentration polarization at the membrane-solution interface. The permeate side was initially filled with deionized water, and the feed side contained 0.2 M methanol and 0.005 M glycerol; 0.005 M glycerol and 0.005 M glucose; or 0.005 M glucose and 0.05 M sucrose. Feed concentrations were chosen based on fluxes and analysis limitations for each analyte. (Experiments with uncoated porous alumina employed lower analyte concentrations to avoid dilution prior to analysis, i.e., 0.1 M methanol, 0.0005 M glycerol, 0.0005 M glucose, and 0.0005 M sucrose.) In each dialysis run, a 1-mL aliquot was removed from both the source and receiving solutions after 5 min, and six more 1-mL aliquots were taken at 10-min intervals for one hour. Flux values were normalized by dividing by the concentration in the feed side.

NF was performed using the cross-flow apparatus represented in Figure 6. The system was pressurized with Ar to 70 psi, and a centrifugal pump circulated the analyte solution through the system and across the membrane. A stainless steel frit

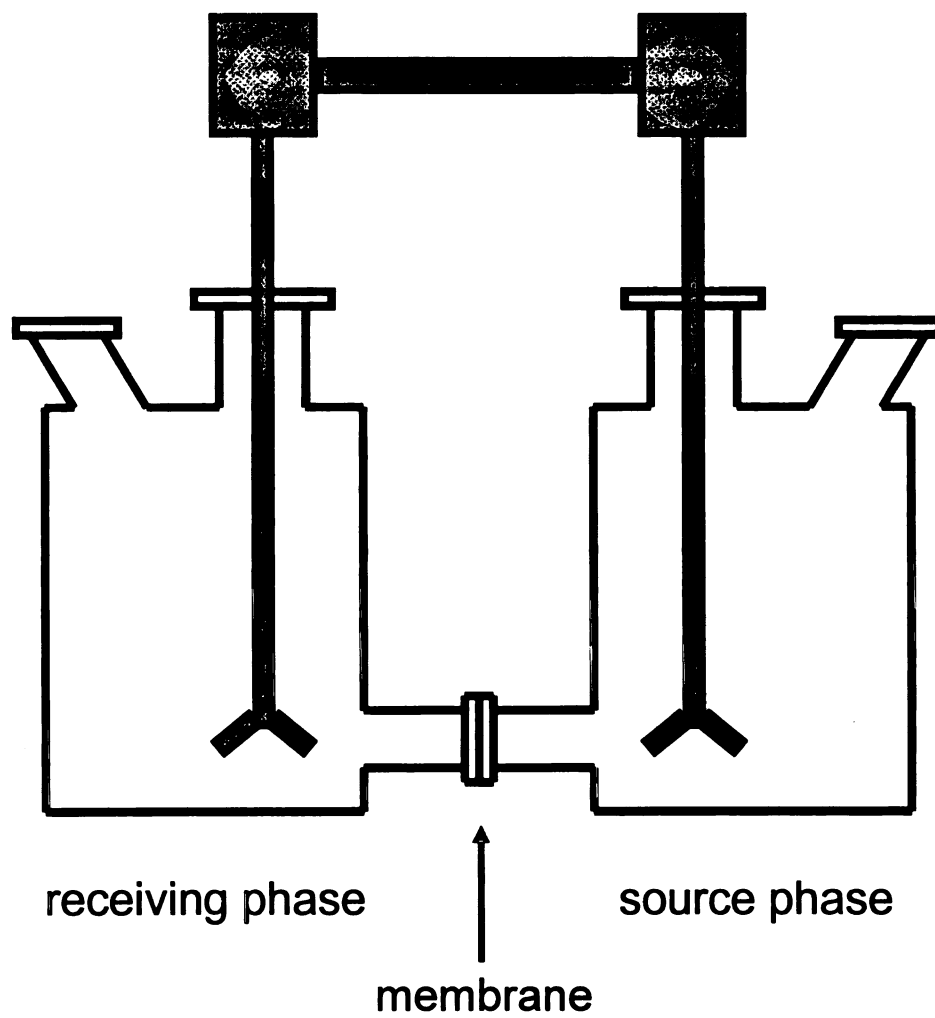


Figure 5. Schematic representation of the cell used in diffusion dialysis.

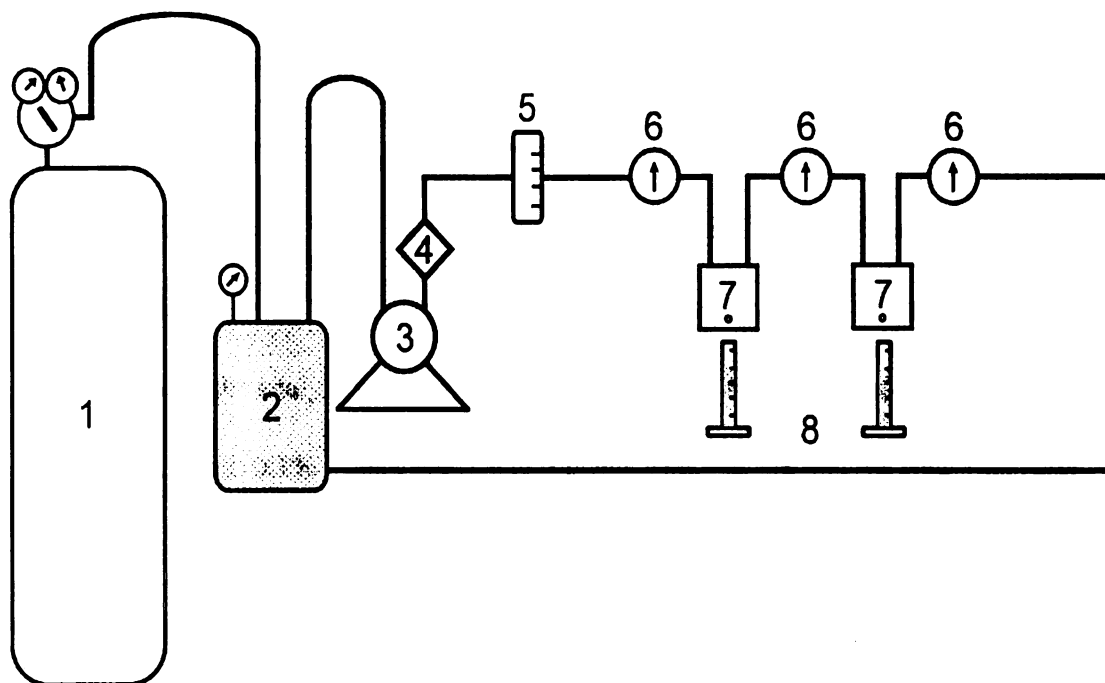


Figure 6. Schematic diagram of the cross-flow nanofiltration apparatus. (1) Ar tank, (2) stainless steel feed tank, (3) centrifugal pump, (4) prefilter, (5) flowmeter, (6) pressure gauges, (7) membrane cells, and (8) graduated cylinders. (Taken from reference 78, with permission from the American Chemical Society, copyright 2003)



(Mott Corporation) was used as a prefilter to remove any rust or particulate matter from the feed stream. The volume of the feed solution (2 L) was about 30-times greater than the total permeate, so the feed composition (0.002 M methanol and 0.0001 M glycerol; or 0.0001 M glycerol, 0.0002 M glucose and 0.005 M sucrose; or 0.0001 M glycerol, 0.0002 M glucose and 0.025 M sucrose) was essentially constant. To avoid concentration polarization, the flow rate across the membrane was kept at 18 mL/min and monitored by a flowmeter located between the pump and membrane cell. The membranes were placed in a home-built stainless steel cell, and the membrane area exposed to the analyte solution was 1.5 cm<sup>2</sup>, which was determined by performing nanofiltration with 0.1% Congo red dye and then measuring the stained area. Several pressure gauges were used to insure that no significant pressure drops occurred across the membrane cells. The permeate was collected with a graduated cylinder after a 10-h equilibration period. Aliquots were taken at 30 min intervals for 1.5 h after the equilibration period, and no significant change in permeate composition was observed after an additional 6 h of NF.

Methanol was analyzed by gas chromatography (Shimadzu, GC-17A, Version 3) using a 30-m-long capillary column (Restek, RTX-BAC1, ID 0.53 mm, film thickness 3  $\mu$ m). In the actual analysis, isopropanol with a specific concentration was chosen as the internal standard. Thus, the calibration curve was made by plotting the methanol concentration as a function of the ratio of methanol peak area to isopropanol peak area (see Figure 7). Each methanol sample taken from diffusion dialysis or nanofiltration was mixed with an equal volume of isopropanol solution and then injected into the GC

for analysis. The injection volume was maintained at 1  $\mu$ L. The initial column temperature stayed at 60  $^{\circ}$ C for 2 min, and then the column was heated to 250  $^{\circ}$ C at a rate of 20  $^{\circ}$ C /min. The temperature was raised to drive all the solvent (water) out of the column.

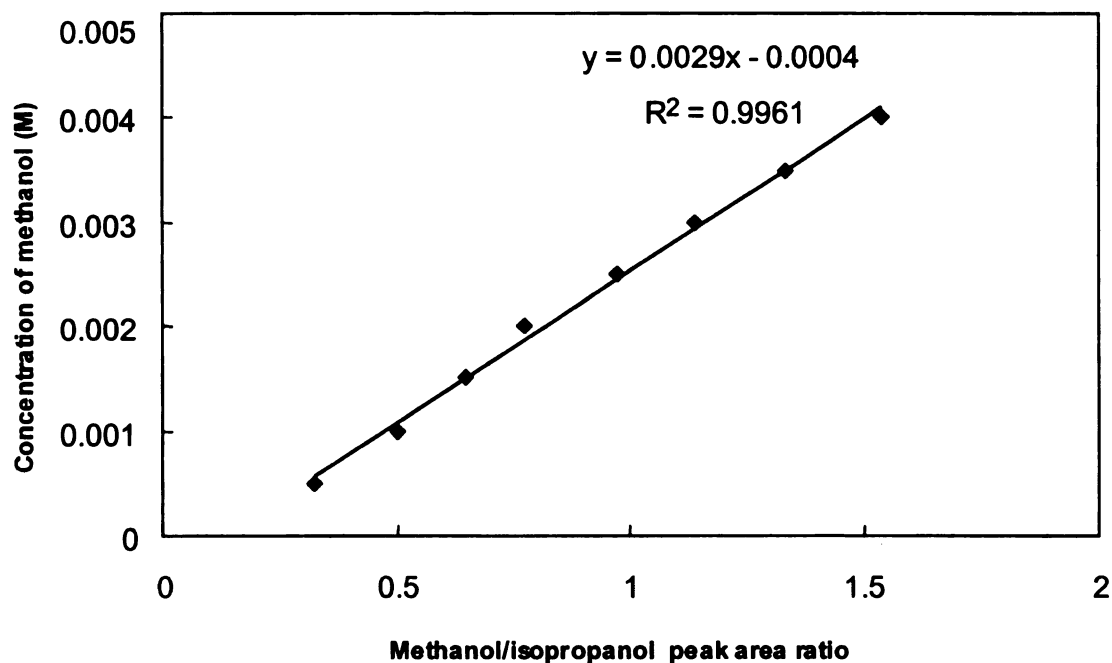


Figure 7. Gas-chromatography calibration curve for methanol.

Glycerol, glucose, and sucrose were analyzed by liquid chromatography (Dionex, DX-600, CarbonPac PA-10 column, 100 mM NaOH eluent) coupled with integrated amperometric detection (Dionex, ED-50). The concentrations were determined using a group of standards bracketing the expected sample concentrations throughout the running period. In this case, standard concentrations versus their corresponding peak

areas were used as calibration plots. A typical chromatogram of a solution containing glycerol, glucose, and sucrose is shown in Figure 8.

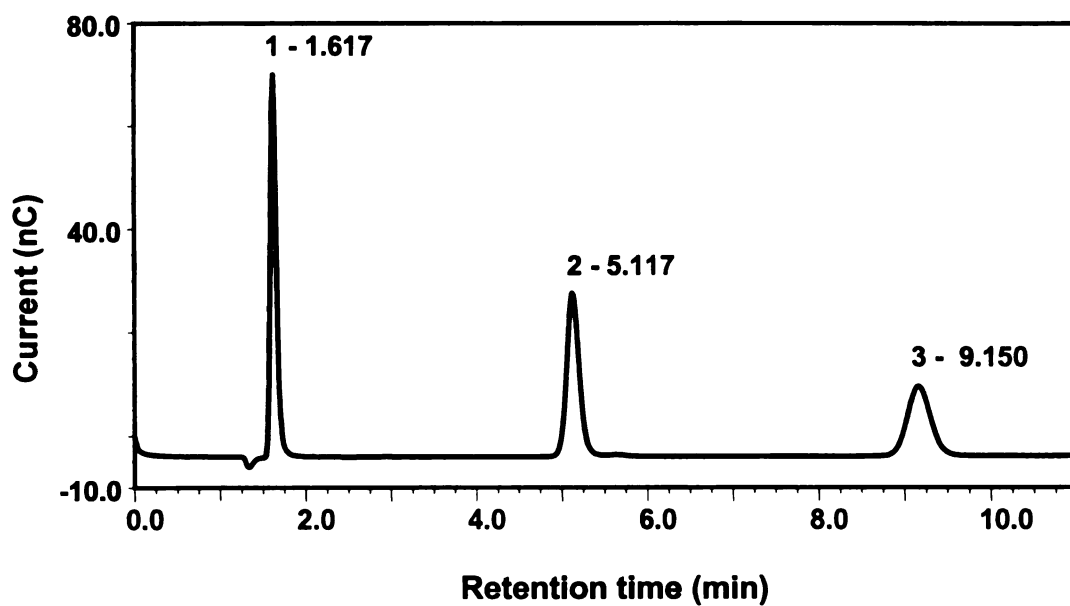


Figure 8. Typical chromatogram of glycerol (peak 1), glucose (peak 2) and sucrose (peak 3) in LC analysis. Numbers next to peak labels are retention times.

## 2.3 Results and Discussion

**2.3.1 Diffusion Dialysis through PSS/PAH Membranes.** To examine the selectivity of PSS/PAH films, we initially employed diffusion dialysis. In these experiments, a porous alumina substrate separates a permeate phase (initially deionized water) from an aqueous source phase that contains the analytes of interest. By monitoring analyte concentrations in the permeate phase as a function of time, one can measure the rate of transport across the membrane. Because analyte concentrations in the permeate phase are negligible compared to those in the source phase, the concentration gradients across the membrane are essentially constant, and permeate-phase concentrations increase linearly with time.

Figure 9 shows permeate-phase concentration as a function of time for the diffusion of glycerol, glucose and sucrose through porous alumina coated with a 7-bilayer PSS/PAH film. Glycerol transport is about 8-times faster than glucose transport, and remarkably, the flux of glucose across the membrane is 150-fold greater than that of sucrose (See Table 3). Corresponding selectivities for bare porous alumina are  $<1.5$ . As all of these analytes are neutral and hydrophilic, selectivity must be based primarily on size.

In ion transport through PSS/PAH films, terminating a membrane with PAH rather than PSS gives a 2-fold increase in the flux of  $\text{SO}_4^{2-}$  and  $\text{Ni}(\text{CN})_4^{2-}$  but has little effect on  $\text{Cl}^-$  transport.<sup>52</sup> In contrast, the flux of sucrose *decreases* 2-fold on going from a 6.5-bilayer ( $[\text{PSS}/\text{PAH}]_6\text{PSS}$ ) to a 7-bilayer ( $[\text{PSS}/\text{PAH}]_7$ ) film (Table 3), and the fluxes of glycerol and glucose also decrease slightly ( $\sim 20\%$ ). The significant

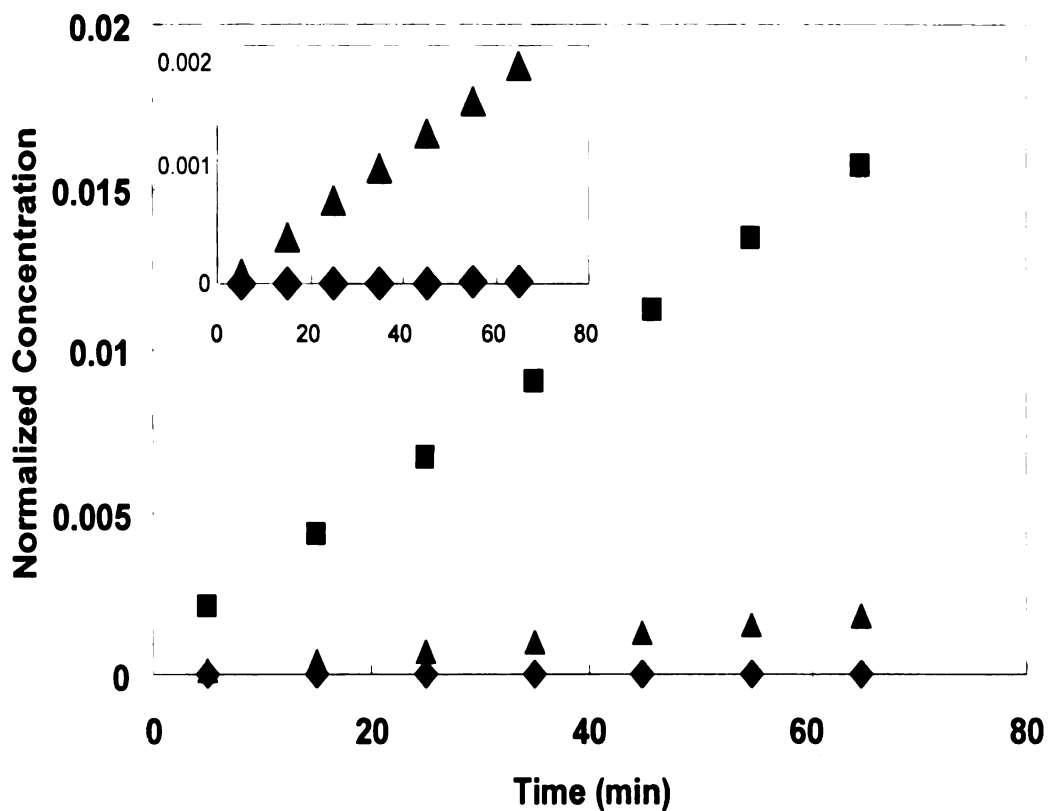


Figure 9. Normalized permeate-phase concentrations of glycerol (squares), glucose (triangles), and sucrose (diamonds) as a function of time in diffusion dialysis through a 7-bilayer PSS/PAH membrane. The inset shows an expanded view for glucose and sucrose. Concentrations were normalized by dividing by the source-phase concentration, and data are from experiments using feed solutions containing 0.005 M glycerol and 0.005 M glucose or 0.005 M glucose and 0.05 M sucrose. Glucose flux was similar for both feed solutions.

decrease in sucrose flux probably results from a tighter surface packing when the top layer is PAH.<sup>79</sup> Surface packing should have little effect on the transport of  $\text{SO}_4^{2-}$  and  $\text{Ni}(\text{CN})_4^{2-}$  because the Stokes' radii of these molecules are less than that of glycerol.<sup>80</sup> Thus, in the transport of divalent anions, changes in Donnan exclusion are the primary result of changing the surface layer to a polycation, and flux increases when terminating films with PAH. In contrast, with neutral molecules Donnan exclusion is not operative, and addition of a PAH layer yields a decrease in flux due to tighter surface packing and/or a thicker membrane.

**Table 3. Normalized Fluxes ( $\text{mol cm}^{-2} \text{ s}^{-1} / \text{M}$ ) and Selectivities in Diffusion****Dialysis through Bare Porous Alumina and Alumina Coated with Polyelectrolyte****Films <sup>a</sup>**

film composition	methanol flux	glycerol flux	glucose flux	sucrose flux	methanol/ glycerol	glycerol/ glucose	glucose/ sucrose
bare	$3.6 \times 10^{-7}$ ( $6 \times 10^{-9}$ )	$2.6 \times 10^{-7}$ ( $8 \times 10^{-9}$ )	$1.8 \times 10^{-7}$ ( $1 \times 10^{-8}$ )	$1.3 \times 10^{-7}$ ( $1 \times 10^{-8}$ )	1.36 (0.05)	1.45 <sup>b</sup> (0.11)	1.35 (0.02)
[PSS/PAH] <sub>6</sub> PSS	$3.5 \times 10^{-7}$ ( $4 \times 10^{-8}$ )	$2.1 \times 10^{-7}$ ( $5 \times 10^{-9}$ )	$2.7 \times 10^{-8}$ ( $2 \times 10^{-9}$ )	$3.4 \times 10^{-10}$ ( $5 \times 10^{-11}$ )	1.96 (0.05)	6.4 (0.4)	80 (7)
[PSS/PAH] <sub>7</sub>	$3.0 \times 10^{-7}$ ( $1 \times 10^{-8}$ )	$1.7 \times 10^{-7}$ ( $5 \times 10^{-9}$ )	$2.2 \times 10^{-8}$ ( $2 \times 10^{-9}$ )	$1.5 \times 10^{-10}$ ( $4 \times 10^{-11}$ )	2.0 (0.1)	7.8 (0.9)	150 (40)
[PSS/PAH] <sub>5</sub> [PAA/PAH]PAA	$2.4 \times 10^{-7}$ ( $2 \times 10^{-8}$ )	$7.3 \times 10^{-8}$ ( $6 \times 10^{-9}$ )	$9.1 \times 10^{-10}$ ( $3 \times 10^{-11}$ )	$< 4.5 \times 10^{-12}$	3.5 (0.6)	75 (20)	>200
[PSS/PAH] <sub>5</sub> [PAA/PAH] <sub>2</sub>	$2.8 \times 10^{-7}$ ( $5 \times 10^{-9}$ )	$1.3 \times 10^{-7}$ ( $2 \times 10^{-8}$ )	$1.4 \times 10^{-8}$ ( $7 \times 10^{-10}$ )	$1.0 \times 10^{-10}$ ( $6 \times 10^{-12}$ )	2.35 (0.03)	10.2 (0.3)	133 (6)

<sup>a</sup>The values in parentheses represent the standard deviations of at least three measurements.

<sup>b</sup>In this case, the selectivity was obtained by dividing the flux of glycerol (from the experiment with methanol/glycerol as the feed solution) by the flux of glucose (from the experiment with glucose and sucrose as the feed solution). In all other cases, analytes were examined competitively in the same solution, and selectivity values are an average of the selectivities in three experiments.

**2.3.2 Diffusion Dialysis through Hybrid PSS/PAH/PAA Membranes.** Simple PSS/PAH membranes are highly selective for glucose over sucrose, but the selectivity for glycerol over glucose is fairly low. Our previous work showed that capping of a 5-bilayer PSS/PAH precursor film with 1.5 bilayers of PAA/PAH yields dramatic increases in  $\text{Cl}^-/\text{SO}_4^{2-}$  selectivity without greatly hindering  $\text{Cl}^-$  flux,<sup>51</sup> so we attempted to use this strategy to enhance selectivity in neutral molecule transport. The flux of glycerol through 5 bilayers of PSS/PAH capped with 1.5 bilayers of PAA/PAH is about one third of that through 6.5-bilayer PSS/PAH films, but glucose flux is 30-fold lower through the capped films. Thus, the overall glycerol/glucose selectivity increases from 6.4 to 75 when using the capping layers (See Figure 10 and Table 3). With films capped with 1.5 bilayers of PAA/PAH, the concentration of sucrose in the permeate is below the detection limit of our analysis ( $\sim 2 \times 10^{-7}$  M), and thus, we can only establish a minimum glucose/sucrose selectivity, which is 200.

The methanol/glycerol selectivity of 3.5 with  $[\text{PSS/PAH}]_5$ ,  $[\text{PAA/PAH}]\text{PAA}$  films is significantly less than that for glycerol over glucose, indicating that the pores in capped membranes are still too large to effectively separate small molecules. This again suggests that the high selectivity in previous ion-transport studies was primarily due to electrostatic effects. The  $\text{Cl}^-/\text{SO}_4^{2-}$  selectivity of  $[\text{PSS/PAH}]_5[\text{PAA/PAH}]\text{PAA}$  films is 70,<sup>51</sup> even though  $\text{SO}_4^{2-}$  has a smaller Stokes' radius (0.23 nm) than glycerol.

The selectivity of capped membranes decreases dramatically when the polyelectrolyte films terminate in PAH rather than PAA (Table 3). Upon going from



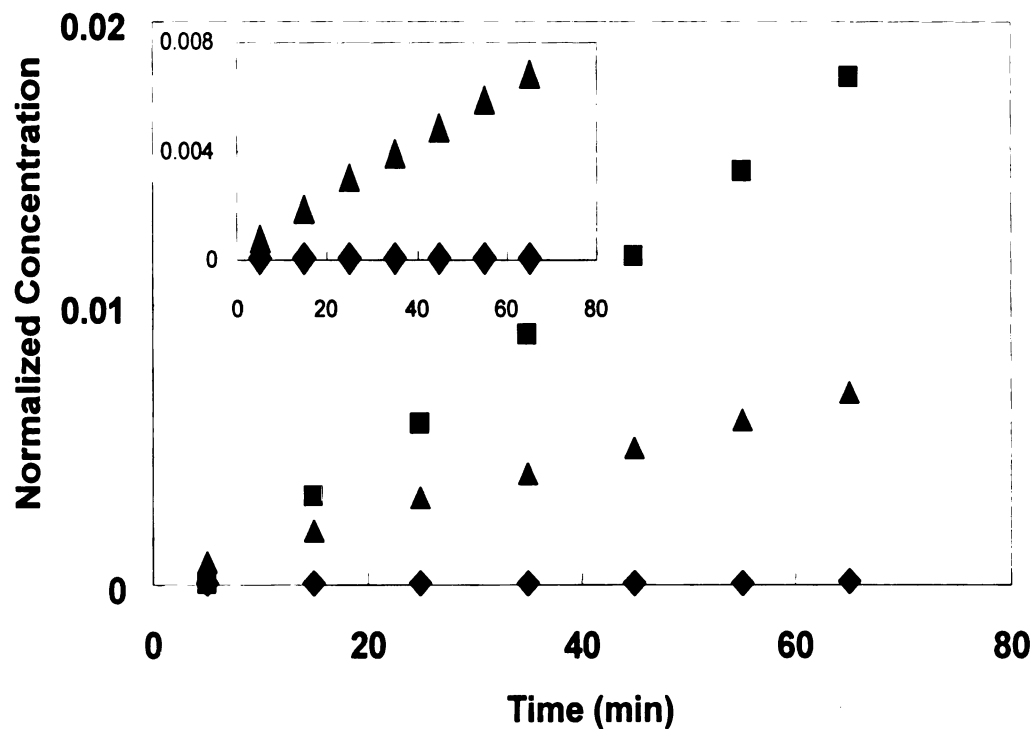


Figure 10. Normalized permeate-phase concentrations of methanol (squares), glycerol (triangles), and glucose (diamonds) as a function of time in a diffusion dialysis experiment with a 5-bilayer PSS/PAH + 1.5-bilayer PAA/PAH film. The inset shows the expanded view of glycerol and glucose transport across the membrane. Glycerol/glucose selectivity is 75. Concentrations were normalized by dividing by the source-phase concentration.

a 1.5-bilayer to a 2-bilayer PAA/PAH cap, glycerol/glucose selectivity decreases from 75 to 10, and methanol/glycerol selectivity decreases from 3.5 to 2.4. Presumably, the film with PAA as the terminal layer has a tighter surface structure than the film with PAH as the top layer. (This trend is opposite to that for PAH and PSS and may reflect the fact that carboxylates are less hydrated than sulfonates.<sup>81</sup>) Although selectivity among small molecules decreases when capped films terminate with PAH, such membranes still exhibit a selectivity of 130 for glucose over sucrose, and glucose flux through [PSS/PAH]<sub>5</sub>[PAA/PAH]<sub>2</sub> films is 15-fold greater than that with a 1.5-bilayer PAA/PAH capping layer. Such wide variations in transport properties should be beneficial for developing membranes for specific applications.

**2.3.3 Nanofiltration with PSS/PAH Membranes.** Table 4 shows percent rejection values, selectivities, and water fluxes (in  $\text{m}^3 \text{m}^{-2} \text{d}^{-1}$ ) from NF experiments with 6.5- and 7-bilayer PSS/PAH membranes and solutions containing several neutral molecules. Water flux through these films is 20-60% lower than our previously published results with 4.5- or 5-bilayer PSS/PAH membranes,<sup>79</sup> presumably because of the greater thickness of 6.5- and 7-bilayer films. However, water fluxes are still similar to those of commercial NF membranes.<sup>82,83</sup>

PSS/PAH membranes show impressive NF selectivities that correlate well with results from diffusion dialysis. In NF, selectivities are calculated according to equation (1),

$$\text{Selectivity} = (100-R_1)/(100-R_2) \quad (1)$$

where R represents percent rejection. Glucose/sucrose selectivities for 6.5-bilayer and 7-bilayer PSS/PAH membranes are 70 and 140, respectively, and the corresponding values in diffusion dialysis are 80 and 150.

Methanol/glycerol and glycerol/glucose selectivities are also similar to those determined in diffusion dialysis. Compared to 7-bilayer PSS/PAH, 6.5-bilayer PSS/PAH membranes exhibit lower selectivities for both glycerol/glucose and glucose/sucrose. However, water fluxes through 7-bilayer and 6.5-bilayer films are about the same. If the higher selectivities of 7-bilayer films were due to tighter surface packing, we would expect to see a slightly lower water flux with these films.

A small difference in water flux could, however, be obscured by the experimental error in our measurements.

**Table 4. Percent Rejections, Water Fluxes (in  $\text{m}^3\text{m}^{-2}\text{d}^{-1}$ ), and Selectivities from NF Experiments with Multilayer Polyelectrolyte Membranes and Solutions Containing Several Neutral Molecules**

film composition	methanol	glycerol	glucose	sucrose	water flux	glycerol/ glucose	glucose/ sucrose
[PSS/PAH] <sub>7</sub>		87±3 <sup>a</sup>	98.3±0.2 <sup>a</sup>	>99.99 <sup>a</sup>	0.90±0.08 <sup>a</sup>	7.7±0.9 <sup>a</sup>	>100 <sup>a</sup>
		97.4±0.4 <sup>b</sup>	99.1±0.2 <sup>b</sup>	99.99±0.01 <sup>b</sup>	0.70±0 <sup>b</sup>	2.8±0.4 <sup>b</sup>	144±31 <sup>b</sup>
	70±5 <sup>c</sup>	88±2 <sup>c</sup>			0.9±0.1 <sup>c</sup>		
[PSS/PAH] <sub>6</sub> PSS	-	90.7±0.4 <sup>a</sup>	97.4±0.6 <sup>a</sup>	99.96±0.01 <sup>a</sup>	0.89±0.05 <sup>a</sup>	3.7±0.7 <sup>a</sup>	68±5 <sup>a</sup>

<sup>a</sup>Experiment conducted with a feed solution containing 0.0001 M glycerol, 0.0002 M glucose, and 0.005 M sucrose. With 7-bilayer films, sucrose concentration in the permeate was near the instrument detection limit.

<sup>b</sup>Experiment conducted with a feed solution containing 0.0001 M glycerol, 0.0002 M glucose, and 0.025 M sucrose.

<sup>c</sup>Experiment conducted with a feed solution containing 0.002 M methanol and 0.0001 M glycerol. Methanol/glycerol selectivity was 2.6±0.9.

In spite of high selectivities, PSS/PAH membranes will probably not be useful for the separation of small organic molecules because of their high rejection values. As shown in Table 4, with 7-bilayer PSS/PAH membranes, methanol, glycerol, glucose and sucrose rejections are 70%, 88%, 98.3% and 99.99%, respectively. Nevertheless, these high rejections could be very beneficial in salt/sugar separations or removal of organic pollutants from water.<sup>75</sup> In the former case, rejection of sugars and high passage of salts should allow selective concentration of oligosaccharides.

The high rejection of sucrose resulted in permeate concentrations near the detection limit of our chromatograph. Because of this, we performed NF with a glycerol/glucose/sucrose solution that contained 0.025 M sucrose rather than 0.005 M sucrose (Table 4). Rejection of both glycerol and glucose increased with the higher sucrose concentration, presumably because sucrose blocked pores at the membrane surface. A decrease in water flux also suggests the presence of adsorbed sucrose, although increased osmotic pressure (9 psi) due to the higher sucrose concentration probably accounts for much of the flux reduction. Sucrose rejection was similar for 0.025 and 0.005 M feed solutions, but rejection was very high in both cases.

**2.3.4 Theory for Modeling of Transport.** Figure 11 shows schematically the concentration profile of a solute diffusing through a multilayer polyelectrolyte/porous alumina membrane. To model diffusion dialysis through such a membrane, we utilized Fick's first law (equation (2)) in both the alumina and the polyelectrolyte film.

$$j_i = -D_i \frac{dc_i}{dx} \quad (2)$$

In this equation,  $j_i$  represents solute flux,  $D_i$  is the solute diffusion coefficient in a particular medium, and  $dc_i/dx$  is the concentration gradient. Because flux is at steady state (see Figures 9 and 10 for evidence of steady-state transport), Fick's law can be rewritten as

$$j_i = -D_i \frac{\Delta c_i}{\Delta x} \quad (3)$$

where  $\Delta x$  is the thickness of either the porous alumina or the polyelectrolyte film and  $\Delta c_i$  represents the total drop in concentration within the appropriate layer. There are also concentration changes at the alumina/polyelectrolyte and polyelectrolyte/feed interfaces due to partitioning into the MPM. (Because the pores in the alumina are large (20-200 nm), there should be no concentration change at the alumina/permeate interface.) With the assumption that the polyelectrolyte film behaves like an assembly of small cylindrical pores,<sup>63,64,84,85</sup> equation (4) describes the relationship between the concentration at the surface of the polyelectrolyte film,  $c_4$ , and the concentration in the feed,  $c_5$  (Figure 11). The partition coefficient,  $\Phi$ , is a function of the ratio of Stokes' radius to pore radius,  $\lambda$ . A similar relationship should exist at the polyelectrolyte/alumina ( $c_3/c_2$ ) interface.

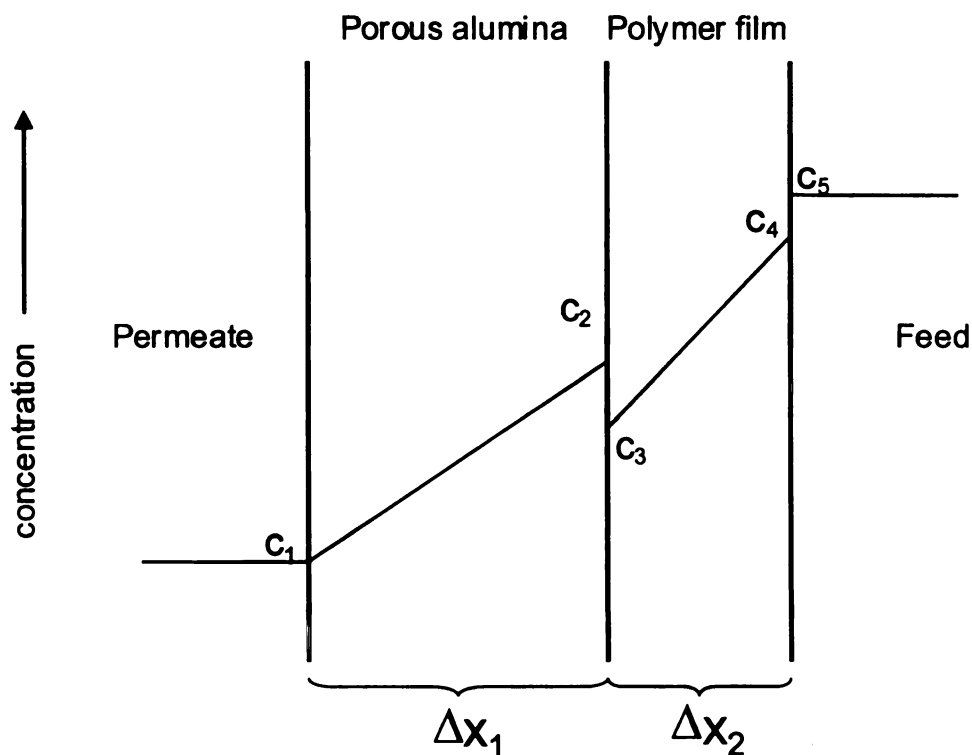


Figure 11. Schematic diagram of the analyte concentration profile in a membrane composed of a polyelectrolyte film on a porous alumina support.

$\Delta x_1$ : thickness of the porous support

$\Delta x_2$ : thickness of the polyelectrolyte film

$c_1$ : analyte concentration in the permeate

$c_2$ : analyte concentration in the alumina support at the support-film interface

$c_3$ : analyte concentration in the film at the support-film interface

$c_4$ : analyte concentration in the film at the film-solution interface

$c_5$ : analyte concentration in the feed

$$\Phi = c_4/c_5 = c_3/c_2 = (1 - \lambda)^2 \quad (4)$$

Assuming that the concentration in the permeate phase,  $c_1$ , is negligible compared to  $c_2$ , we can calculate  $c_2$  from the experimental flux value using equation (5). We obtained  $D_1$ , the diffusion coefficient in the porous alumina, from diffusion dialysis data with a bare porous alumina support, and  $\Delta x_1$  is thickness of the alumina (~60  $\mu\text{m}$ ).

$$c_2 = j_i \Delta x_1 / D_1 \quad (5)$$

For transport through the polyelectrolyte film, substitution of equation (4) and equation (5) into equation (3) plus rearrangement yields the expression for flux in equation (6).

$$j_i = \frac{c_5}{\frac{\Delta x_2}{D_2(1-\lambda)^2} + \frac{\Delta x_1}{D_1}} \quad (6)$$

However,  $D_2$ , the diffusion coefficient in the MPM, is a function of the hindrance factor for diffusion in small pores,  $K_{i,d}$ , the film porosity,  $\varepsilon$ , and the diffusion coefficient in free solution,  $D_{inf}$ , as shown in equation (7).<sup>65</sup>

$$D_2 = D_{inf} K_{i,d} \varepsilon \quad (7)$$

Using correlations for  $K_{i,d}$  as a function of  $\lambda$  (see below), one can write the flux  $j_i$  through the MPM in terms of two variables,  $\lambda$  and  $\varepsilon$ . To estimate film porosity, we utilized measurements of water flux in NF. Assuming that all the pores in a film have the same radii, volume flux in NF can be described by equation (8), where  $J_v$  is the volume flux,  $r$  is the pore radius,  $\Delta P$  is the pressure drop across the film,  $\eta$  is the solvent viscosity, and  $\tau$  is the pore tortuosity. (For straight cylindrical pores, the tortuosity is equal to unity.)



$$J_v = \frac{r^2 \varepsilon \Delta P}{8 \eta \tau \Delta x} \quad (8)$$

With water-flux data from NF and solute-flux data from diffusion dialysis, equations (6) (with substitution of equation (7)) and (8) can be solved iteratively for  $r$  and  $\varepsilon$  if the radius of the solute is known. In our actual calculation of  $r$ , we first assumed a value of  $r$  and calculated  $\varepsilon$  from equation (8) and  $D_2$  from equation (7) and the correlations given below for  $K_{i,d}$ . Finally, we calculated flux from equation (6). We optimized the value assumed for  $r$  to minimize the sum of least squares of percent error in the fluxes of methanol, glycerol, glucose and sucrose.

In the case of NF, the expression for solute flux contains both diffusive and convective terms. The treatment that we followed to simulate transport is similar to that developed by Bowen et al.<sup>65</sup> Addition of convection to Fick's law yields equation (9), where  $J_v$  is the volume flux of the solvent.

$$j_i = -D_i \frac{dc_i}{dx} + K_{i,c} c_i J_v \quad (9)$$

The hindered nature of convection and diffusion inside membrane pores is accounted for by  $K_{i,c}$ , the hindrance factor for convection, and  $K_{i,d}$  (equation (7) for  $D_2$ ), the hindrance factor for diffusion, which are functions of  $\lambda$ . If one assumes a homogenous velocity across very small membrane pores,  $K_{i,d}$  and  $K_{i,c}$  are respectively equivalent to  $K^{-1}(\lambda, 0)$ , the enhanced drag coefficient, and  $G(\lambda, 0)$ , the lag coefficient.<sup>64,65</sup> Bungay and Brenner fitted the enhanced drag and lag coefficients to equations (10) and (11).<sup>86,87</sup> Other correlations for drag and lag coefficients gave similar results in our simulations.<sup>65,86</sup>

$$K^{-1}(\lambda,0) = 6\pi / \left\{ \frac{9}{4} \pi^2 \sqrt{2} (1-\lambda)^{-2.5} \left[ 1 - \frac{73}{60} (1-\lambda) + \frac{77293}{50400} (1-\lambda)^2 \right] - 22.5083 - 5.6117\lambda - 0.3363\lambda^2 - 1.216\lambda^3 + 1.647\lambda^4 \right\} \quad (10)$$

$$G(\lambda,0) = \left\{ \frac{9}{4} \pi^2 \sqrt{2} (1-\lambda)^{-2.5} \left[ 1 + \frac{7}{60} (1-\lambda) - \frac{2227}{50400} (1-\lambda)^2 \right] + 4.0180 - 3.9788\lambda - 1.9215\lambda^2 + 4.392\lambda^3 + 5.006\lambda^4 \right\} \frac{K^{-1}(\lambda,0)}{12\pi} \quad (11)$$

Integration of equation (9) over the polyelectrolyte film with the boundary conditions listed in equation (12) ( $c_{i,f}$  and  $c_{i,p}$  are the solute concentrations in the feed and permeate, respectively) yields the expression for rejection,  $R$ , in equation (13). In this equation, the Peclet number,  $Pe_m$  is defined as shown in equation (14).

$$c_{i,x=0} = \Phi c_{i,f} \text{ and } c_{i,x=\Delta x} = c_{i,p} \quad (12)$$

$$R = 1 - \frac{c_{i,p}}{c_{i,f}} = 1 - \frac{K_{i,c} \Phi}{1 - \exp(-Pe_m)(1 - K_{i,c})} \quad (13)$$

$$Pe_m = \frac{K_{i,c}}{K_{i,d}} \frac{J_v \Delta x}{D_{i,\infty} \varepsilon} \quad (14)$$

Equations (13) and (14) provide an expression for rejection as a function of  $\lambda$  and  $\varepsilon$ .

In the actual procedure for determining the porosity and pore radius from NF data, we first assumed a value for pore size and calculated porosity from equation (8). We then determined the hindrance factors for both diffusion and convection using equations (10) and (11), and subsequently calculated rejection with equation (13). Iterations on this procedure yielded a best-fit pore radius through minimization of the sum of least squares for the percent error in  $(1-R)$  for methanol, glycerol, and glucose.

We note that for cross-flow NF, we assumed partition equilibrium only at the feed-side interface. The polyelectrolyte/alumina interface is not stirred so we assumed that the concentration on the alumina side of this interface is the same as the

concentration in the polyelectrolyte. We also neglected mass-transport resistance due to the alumina support. This is an appropriate assumption in NF because water flux through bare alumina is >100 times larger than flux through PSS/PAH-coated alumina. In diffusion dialysis, however, the alumina support provides a significant resistance to mass transport.

**2.3.5 Determination of Effective Pore Sizes.** The models described above allow estimation of effective pore sizes and porosity in polyelectrolyte films, and these parameters will be important for prediction of selectivity and flux in specific separations. Table 5 shows simulated fluxes for diffusion dialysis and the important variables used to calculate these fluxes. Minimization of the percent error in the flux of the different solutes gave an effective pore radius of 0.53 nm and a porosity of 1.8%. Calculated fluxes of all four solutes were within at least 32% of the measured values. However, effective pore size depends greatly on the value of  $D_{\text{inf}}$  chosen for the calculation. We utilized the effective diffusion coefficient (uncorrected for porosity) in porous alumina as the value of  $D_{\text{inf}}$ . If we correct this value for the alumina porosity determined from NF experiments (21%), the calculated pore size in the polyelectrolyte film decreases to 0.45 nm and porosity increases to 2.5%.<sup>88</sup> We utilized the uncorrected value for the diffusion coefficient because we thought that

**Table 5. Parameters and Fluxes ( $J$ , mol cm<sup>-2</sup> s<sup>-1</sup>) Relevant to the Simulation of Diffusion Dialysis through a 7-bilayer PSS/PAH Membrane Assuming a Pore Radius of  $5.28 \times 10^{-8}$  cm <sup>a</sup>**

	$\lambda$	$(1-\lambda)^2$	$D_{inf.}(cm^2s^{-1})$	$D_2(cm^2s^{-1})$	$J_{calculated}$	$J_{measured}$
methanol	0.30	0.49	$2.1 \times 10^{-6}$	$1.6 \times 10^{-8}$	$6.3 \times 10^{-8}$	$6.0 \times 10^{-8}$
glycerol	0.49	0.26	$1.6 \times 10^{-6}$	$4.8 \times 10^{-9}$	$8.0 \times 10^{-10}$	$8.7 \times 10^{-10}$
glucose	0.67	0.11	$1.1 \times 10^{-6}$	$9.9 \times 10^{-10}$	$1.5 \times 10^{-10}$	$1.1 \times 10^{-10}$
sucrose	0.89	0.012	$8.0 \times 10^{-7}$	$3.7 \times 10^{-11}$	$7.2 \times 10^{-12}$	$7.3 \times 10^{-12}$

<sup>a</sup>A porosity of 1.8% was calculated from equation (8) using nanofiltration data at 70 psi that yielded a water flux of  $0.001 \text{ cm}^3 \text{ cm}^{-2} \text{ s}^{-1}$ . The polyelectrolyte film thickness was assumed to be 30 nm based on ellipsometric measurements.

**Table 6. Parameters and Rejections Calculated in the Simulation of Nanofiltration with a 7-bilayer PSS/PAH Membrane Assuming a Pore Radius of  $4.2 \times 10^{-8}$  cm <sup>a</sup>**

	$\lambda$	$(1-\lambda)^2$	$K^{-1}$	$K_{i,c}$	calculated % rejection.	measured % rejection.
methanol	0.37	0.39	0.31	0.89	61.4	$70 \pm 5$
glycerol	0.62	0.15	0.078	0.76	87.5	$88 \pm 2$
glucose	0.85	0.024	0.0067	0.60	98.5	$98.3 \pm 0.2$
sucrose	>1	-	-	-	100	$99.99 \pm 0.01$

<sup>a</sup>A porosity of 2.8% was calculated from equation (8) and nanofiltration data at 70 psi that yielded a water flux of  $0.001 \text{ cm}^3 \text{ cm}^{-2} \text{ s}^{-1}$ . The polyelectrolyte film thickness was assumed to be 30 nm.



diffusion through the film would not occur to nonporous areas of the alumina surface. (This assumption implies that lateral diffusion at the polyelectrolyte/alumina interface is insignificant.) The calculated diffusion coefficient,  $D_2$ , for sucrose (MW = 342) is similar to that measured by Ibarz et al. for fluorescein (MW = 332) diffusion through annealed polyelectrolyte capsules.<sup>89</sup>

Simulation of NF (Table 6) resulted in a pore size of 0.42 nm and a porosity of 2.8%. Calculated rejections were within 12% of measured values. We should note that the simulations assume a uniform pore size, while, in fact, there is certainly a distribution of pore sizes, and thus, effective pore sizes are only rough approximations. This may explain why a small amount of sucrose passes through the membrane even though its Stokes' radius is larger than the effective pore radius. The calculated pore size in NF is 0.1 nm less than the value from diffusion dialysis, and this may reflect the approximate nature of the simulations or the choice of diffusion coefficient in the diffusion dialysis calculation. However, compaction due to the pressure applied in NF could also decrease pore sizes.

Effective pore sizes are consistent with the fact that the approximate molecular weight cutoff (90% rejection in NF) of these membranes is around 92, the molecular weight of glycerol. The Stokes' radius of glycerol is 0.26 nm, and molecules larger than this should be highly rejected from the membrane, primarily due to the partition coefficient, which is a function of the ratio of Stokes' radius to pore radius (equation (4)). In fact, the NF model suggests that partitioning is the primary factor behind

selectivity with the molecules examined, although there is a small effect from hindered convection.

One of the reasons for performing this work was to determine if there was a size-based selectivity in ion separations, e.g.,  $\text{Cl}^-$  and  $\text{SO}_4^{2-}$ . Because the Stokes' radii of these ions are significantly less than the pore radius, size selectivity should be <2 with PSS/PAH membranes. However, other polyelectrolyte systems may pack more tightly and allow for size discrimination among small ions. Additionally, electrostatic interactions between ions and polyelectrolytes can result in selective diffusion, as shown by Farhat and Schlenoff.<sup>55,56</sup> Our future work aims at controlling pore size in MPMs by carefully selecting constituent polyelectrolytes.

## **Chapter 3**

### **Conclusions and Future Work**

MPMs are highly selective for neutral molecules in both diffusion dialysis and NF. These membranes demonstrate glucose/sucrose selectivity as high as 150, and size exclusion is the main factor behind such selectivities. Modeling of solute and solvent fluxes as well as rejection values suggests that PSS/PAH membranes contain pores with radii of 0.4 to 0.5 nm. The high rejections of glucose and sucrose by PSS/PAH membranes along with a high water flux suggest that these materials may be applicable in salt/sugar separations or removal of organic pollutants from water. In contrast to neutral molecules, however, selective transport of small ions such as  $\text{Cl}^-$  and  $\text{SO}_4^{2-}$  through PSS/PAH films should not be based on size because the Stokes' radii of these ions are significantly smaller than film pores.

Although this thesis clearly demonstrates the potential of MPMs, further work will be necessary prior to practical separations with these materials. The porous alumina support for MPMs is quite fragile, so large-scale applications will likely require methods for preparation of films on polymeric substrates. These methods will need to be optimized to achieve both high water flux and high selectivities. For separation of sugars in NF, as we already suggested, we need to lower rejections substantially while maintaining high selectivities. This could be achieved by careful selection of constituent polyelectrolytes or tuning of deposition conditions.



## References:

- (1) Ding, Y.; Bikson, B.; Nelson, J. K. *Macromolecules* **2002**, *35*, 912.
- (2) Clausi, D. T.; Koros, W. J. *J. Membr. Sci.* **2000**, *167*, 79.
- (3) Mulder, M. *Basic Principles of Membrane Technology*; Kluwer Academic Publishers: Dordrecht, The Netherlands, 1996.
- (4) Xu, Y.; Lebrun, R. E. *Desalination* **1999**, *122*, 95.
- (5) Tsuru, T.; Izumi, S.; Yoshioka, T.; Asaeda, M. *AIChE J.* **2000**, *46*, 565.
- (6) Paul, D. H. *Ultrapure Water*; Tall Oaks Publishing, 1998.
- (7) Van den Berg, G. B.; Smolders, C. A. *J. Membr. Sci.* **1989**, *40*, 149.
- (8) Nakao, S.; Wijmans, J. G.; Smolders, C. A. *J. Membr. Sci.* **1986**, *26*, 165.
- (9) Kesting, R. E.; Fritzche, A. K. *Polymeric Gas Separation Membranes*; John Wiley & Sons: New York, 1993.
- (10) Pinnau, I.; Koros, W. J. *Ind. Eng. Chem. Res.* **1991**, *30*, 1837.
- (11) Pinnau, I.; Koros, W. J. *J. Appl. Polym. Sci.* **1992**, *46*, 1195.
- (12) Tieke, B.; Ackern, F. van.; Krasemann, L.; Toutianoush, A. *Eur. Phys. J. E* **2001**, *5*, 29.
- (13) Bruinsma, P. J.; Stroeve, P.; Hoffmann, C. L.; Rabolt, J. F. *Thin Solid Films* **1996**, *284-285*, 713.
- (14) Maximychev, A. V.; Matyukhin, V. D.; Stepina, N. D.; Yanusova, L. G. *Thin Solid Films* **1996**, *284-285*, 866.
- (15) Seufert, M.; Fakirov, C.; Wegner, G. *Adv. Mater.* **1995**, *7*, 52.
- (16) Conner, M. D.; Janout, V.; Kudelka, I.; Dedek, P.; Zhu, J.; Regen, S. L. *Langmuir* **1993**, *9*, 2389.
- (17) Ulman, A. *An Introduction to Ultrathin Organic Films*; Academic Press: Boston, 1991.

- (18) Tieke, B. *Adv. Mater.* **1991**, *11*, 532.
- (19) Lvov, Y.; Decher, G.; Sukhorukov, G. *Macromolecules* **1993**, *26*, 5396.
- (20) Decher, G. *Science* **1997**, *277*, 1232.
- (21) Decher, G.; Hong, J. D.; Schmitt, J. *Thin Solid Films* **1992**, *210-211*, 831.
- (22) Stroeve, P.; Vasquez, V.; Coelho, M. A. N.; Rabolt, J. F. *Thin Solid Films* **1996**, *284-285*, 708.
- (23) Liu, C.; Martin, C. R. *Nature* **1991**, *352*, 50.
- (24) von Klitzing, R.; Möhwald, H. *Thin Solid Films* **1996**, *352*, 284.
- (25) Han, S.; Lindholm-Sethson, B. *Electrochim. Acta* **1999**, *45*, 845.
- (26) Ichinose, I.; Mizuki, S.; Ohno, S.; Shiraishi, H.; Kunitake, T. *Polym. J.* **1999**, *31*, 1065.
- (27) Delcorte, A.; Bertrand, P.; Wischerhoff, E.; Laschewsky, A. *Langmuir* **1997**, *13*, 5125.
- (28) Möhwald, H. *Colloids Surf. A: Physicochem and Eng. Aspects* **2000**, *171*, 25.
- (29) Lvov, Y.; Ariga, K.; Ichinose, I.; Kunitake, T. *J. Am. Chem. Soc.* **1995**, *117*, 6117.
- (30) Russell, R. J.; Sirkar, K.; Pishko, M. V. *Langmuir* **2000**, *16*, 4052.
- (31) Caruso, F.; Niikura, K.; Furlong, D. N.; Okahata, Y. *Langmuir* **1997**, *13*, 3422.
- (32) Mendelsohn, J. D.; Barrett, C. J.; Chan, V. V.; Pal, A. J.; Mayes, A. M.; Rubner, M. F. *Langmuir* **2000**, *16*, 5017.
- (33) Shiratori, S. S.; Rubner, M. F. *Macromolecules* **2000**, *33*, 4213.
- (34) Yoo, D.; Shiratori, S. S.; Rubner, M. F. *Macromolecules* **1998**, *31*, 4309.
- (35) Harris, J. J.; Bruening, M. L. *Langmuir* **2000**, *16*, 2006.
- (36) Ladam, G.; Schaad, P.; Voegel, J. C.; Schaaf, P.; Decher, G.; Cuisiner, F. *Langmuir* **2000**, *16*, 1249.

- (37) Lösche, M.; Schmitt, J.; Decher, G.; Bouwman, W. G.; Kjaer, K. *Macromolecules* **1998**, *31*, 8893.
- (38) Steitz, R.; Leiner, V.; Siebrecht, R.; von Klitzing, R. *Colloids Surf. A: Physicochem. Eng. Aspects* **2000**, *163*, 63.
- (39) Mendelsohn, J. D.; Yang, S. Y.; Hiller, J. A.; Hochbaum, A. I.; Rubner, M. F. *Biomacromolecules* **2003**, *4*, 96.
- (40) Yang, S. Y.; Mendelsohn, J. D.; Rubner, M. F. *Biomacromolecules* **2003**, *4*, 987.
- (41) Zhou, P.; Samuelson, L.; Alva, K.S.; Chen, C.; Blumstein, R. B.; Blumstein, A. *Macromolecules* **1997**, *30*, 1577.
- (42) Ackern, F. Van.; Krasemann, L.; Tieke, B. *Thin Solid Films* **1998**, *329*, 762.
- (43) Leväsalmi, J. M.; McCarthy, T. J. *Macromolecules* **1997**, *30*, 1752.
- (44) Meier-Haack, J.; Lenk, W.; Lehmann, D.; Lunkwitz, K. *J. Membr. Sci.* **2001**, *184*, 233.
- (45) Krasemann, L.; Tieke, B. *J. Membr. Sci.* **1998**, *150*, 23.
- (46) Krasemann, L.; Tieke, B. *J. Membr. Sci.* **2001**, *181*, 221.
- (47) Graul, T. W.; Schlenhoff, J. B. *Anal. Chem.* **1999**, *71*, 4007.
- (48) Müller, M.; Rieser, T.; Lunkwitz, K.; Meier-Haack, J. *Macromol. Rapid Commun.* **1999**, *20*, 607.
- (49) Rieser, T.; Lunkwitz, K.; Berwald, S.; Meier-Haack, J.; Kessler, B.; Simon, F. *Polym. Mater. Sci. Eng.* **1997**, *77*, 351.
- (50) Bruening, M. L.; Harris, J. J.; Sullivan, D. M. *Polym. Mater. Sci. Eng.* **2001**, *85*, 525.
- (51) Stair, J. L.; Harris, J. J.; Bruening, M. L. *Chem. Mater.* **2001**, *13*, 2641.
- (52) Harris, J. J.; Stair, J. L.; Bruening, M. L. *Chem. Mater.* **2000**, *12*, 1941.
- (53) Krasemann, L.; Tieke, B. *Langmuir* **2000**, *16*, 287.
- (54) Sullivan, D. M.; Bruening, M. L. *J. Am. Chem. Soc.* **2001**, *123*, 11805.

- (55) Farhat, T. R.; Schlenoff, J. B. *Langmuir* **2001**, *17*, 1184.
- (56) Farhat, T. R.; Schlenoff, J. B. *J. Am. Chem. Soc.* **2003**, *125*, 4627.
- (57) Dai, J.; Jensen, A. W.; Mohanty, D. K.; Erndt, J.; Bruening, M. L. *Langmuir* **2001**, *17*, 931.
- (58) Balachandra, A. M.; Dai, J.; Bruening, M. L. *Macromolecules* **2002**, *35*, 3171.
- (59) Dai, J.; Balachandra, A. M.; Lee, J. I.; Bruening, M. L. *Macromolecules* **2002**, *35*, 3164.
- (60) van der Horst, H. C.; Timmer, J. M. K.; Robbertsen, T.; Leenders, J. *J. Membr. Sci.* **1995**, *104*, 205.
- (61) Tsuru, T.; Nakao, S.; Kimura, S. *J. Chem. Eng. Jpn* **1991**, *24*, 511.
- (62) Wang, X. L.; Tsuru, T.; Nakao, S.; Kimura, S. *J. Membr. Sci.* **1995**, *103*, 117.
- (63) Wang, X. L.; Tsuru, T.; Togou, M.; Nakao, S.; Kimura, S. *J. Chem. Eng. Jpn* **1995**, *28*, 186.
- (64) Bowen, W. R.; Mukhtar, H. *J. Membr. Sci.* **1996**, *112*, 263.
- (65) Bowen, W. R.; Mohammad, A. W.; Hilal, N. *J. Membr. Sci.* **1997**, *126*, 91.
- (66) Caruso, F.; Yang, W.; Trau, D.; Renneberg, R. *Langmuir* **2000**, *16*, 8932.
- (67) Shi, X.; Caruso, F. *Langmuir* **2001**, *17*, 2036.
- (68) Qiu, X.; Leporatti, S.; Donath, E.; Möhwald, H. *Langmuir* **2001**, *17*, 5375.
- (69) Duchesne, T. A.; Brown, J. Q.; Guice, K. B.; Lvov, Y.; McShane, M. J. *Sensors and Materials* **2002**, *14*, 293.
- (70) Lvov, Y.; Antipov, A. A.; Mamedov, A.; Möhwald, H.; Sukhorukov, G. B. *Nano Letters* **2001**, *1*, 125.
- (71) Kato, N.; Schuetz, P.; Fery, A.; Caruso, F. *Macromolecules* **2002**, *35*, 9780.
- (72) Bohdziewicz, J.; Bodzek, M.; Wasik, E. *Desalination* **1999**, *121*, 139.
- (73) Yaroshchuk, A.; Staude, E. *Desalination* **1992**, *86*, 115.

- (74) Matsubara, Y.; Iwasaki, K.; Nakajima, M.; Nabetani, H.; Nakao, S. *Biosci. Biotech. Biochem.* **1996**, *60*, 421.
- (75) Wang, X.; Zhang, C.; Ouyang, P. *J. Membr. Sci.* **2002**, *204*, 271.
- (76) Bowen, W. R.; Mohammad, A. W. *AIChE J.* **1998**, *44*, 1799.
- (77) Derlacki, Z. J.; Easteal, A. J.; Edge, A. V. J.; Woolf, L. A. *J. Phys. Chem.* **1985**, *89*, 5318.
- (78) Decher, G.; Lvov, Y.; Schmitt, J. *Thin Solid Films* **1994**, *244*, 772.
- (79) Stanton, B. W.; Harris, J. J.; Miller, M. D.; Bruening, M. L. *Langmuir* **2003**, *19*, 7038.
- (80) *Sulfate has a Stokes' radius of 0.23 nm, and based on our previous studies of  $\text{SO}_4^{2-}$  and  $\text{Ni}(\text{CN})_4^{2-}$  transport through bare porous alumina,  $\text{Ni}(\text{CN})_4^{2-}$  should have a similar radius.*<sup>51</sup>
- (81) Davis, T. A.; Genders, J. D.; Pletcher, D. *A First Course in Ion Permeable Membranes*; The Electrochemical Consultancy, 1997.
- (82) Performance characteristics of some commercially available membranes can be found at [www.dow.com/liquidseps/pc/nfe.htm](http://www.dow.com/liquidseps/pc/nfe.htm) and [www.osmonics.com](http://www.osmonics.com).
- (83) Bhattacharyya, D.; Williams, M. E.; Ray, R. J.; McCray, S. B. *Membrane Handbook*; Van Nostrand Reinhold: New York, 1992, p 263.
- (84) Wang, X. L.; Tsuru, T.; Togou, M.; Nakao, S.; Kimura, S. *J. Membr. Sci.* **1997**, *135*, 19.
- (85) Nakao, S.; Kimura, S. *J. Chem. Eng. Jpn* **1982**, *15*, 200.
- (86) Deen, W. M. *AIChE J.* **1987**, *33*, 1409.
- (87) Bungay, P. M.; Brenner, H. *Int. J. Multiphase Flow* **1973**, *1*, 25.
- (88) *After correcting for porosity, diffusion coefficients measured in porous alumina are about 60% of those literature values listed in Table 1. This may reflect the fact that diffusion coefficients in alumina were not measured at infinite dilution. If the diffusion coefficients in Table 1 are used in simulations, we obtain a pore radius of 0.44 nm and a porosity of 2.6%. The choice of diffusion coefficients has little effect on simulations of NF, however.*

(89) Ibarz, G.; Dähne, L.; Donath, E.; Möhwald H. *Chem. Mater.* **2002**, *14*, 4059.



MICHIGAN STATE UNIVERSITY LIBRARIES



3 1293 02470 8780